CLM - P 558

CLM - P 558

UKAEA

Preprint

OPERATION AND PERFORMANCE OF OPTICALLY PUMPED ROTO-VIBRATIONAL MOLECULAR LASERS AT LOW TEMPERATURES

J M GREEN

CULHAM LABORATORY
Abingdon Oxfordshire

1979

CLM-P558

OPERATION AND PERFORMANCE OF OPTICALLY PUMPED ROTO-VIBRATIONAL MOLECULAR LASERS AT LOW TEMPERATURES

J.M. Green

UKAEA Culham Laboratory,
Abingdon, Oxon OX14 3DB.

ABSTRACT

The low temperature operation and performance of the 19 μm OCS and 16 μm CF_4 CO_2 laser-pumped lasers is reported. Both in terms of output energy and operating pressure the performance of these lasers is shown to greatly improve with decreasing temperature in agreement with the predictions of a simple theoretical model.

(Submitted for publication in J.Phys.D, Appl.Phys.)

October, 1978.

Recent experimental results have demonstrated that by operating optically pumped roto-vibrational molecular lasers (OPMLs) at low temperatures, their performance can be greatly improved.[1,2,3,4,5] Such improvements are particularly important in view of the potential applications of these lasers in a variety of photochemical processes based on selective vibrational excitation of molecules. In this paper a liquid nitrogen (LN_2) cooled OPML cell is described, and the performance of the device is illustrated through a parametric study of two OPMLs pumped by a CO_2 laser, the carbonyl sulphide (OCS) 19 μm laser[6] pumped by the P(22) 9.2 μm line and the 'Freon 14' (CF_4) 16 μm laser[3] pumped by the R(12) 9.6 μm line. In both cases we report the highest specific output energies (J cm^{-3} $Torr^{-1}$ per joule of pump energy injected into the OPML cell) and operating pressures so far achieved in these lasers. These results were achieved at the lowest operating temperatures consistent with the vapour pressure limitations of the lasant gas.

Fig.1 shows the design of the cooled OPML cell. The design is based around the use of a square section tube to contain the lasant gas. The tube of length 1m and internal side 12 mm was made by drawing a circular copper tube over a specially made plug to produce mirror-like internal surfaces. The tube was terminated at one end by an internally mounted mirror, and at the other end by a salt (KBr) window which was held by Brewster's angle to the axis of the tube in a mount which also included an entrance port for filling the cell and monitoring its pressure. Both (room temperature) end pieces were thermally isolated from the square sectioned tube by short lengths of thin wall stainless steel tubing which were vacuum brazed one at each end.

For many molecular gases of interest, saturated vapour pressures (SVPs) lie in the typical OPML operating pressure range (0.1 to 10 Torr) at temperatures ≤ 200K, with some (eg CF_4) as low as 100K. Consequently LN_2 was used as the coolant rather than a conventional low temperature freezing mixture. In order, however, to avoid the creation of 'cold spots' but rather to create a uniform temperature along the length of the OPML cell during LN_2 cooling, the square section tube was clamped between two massive brass blocks to increase the thermal mass and thermal conductivity along the bar. When assembled as shown in Fig.1 the blocks formed a square section of side 100 mm and provided the high thermal capacity and conductivity required for good temperature stability and uniformity. Thermal insulation of the brass blocks

was achieved using 20 mm thick fibreglass on three sides and a 25 mm thick resin bonded epoxy block on top. A number of channels were machined along the length of each of the brass blocks and, through holes in the resin bonded block, these channels were connected to a tank as shown in Fig.1. In this way, LN_2 added to the tank (typically in 5ℓ quantities) was distributed between the channels in a uniform manner.

The OPML cavity comprised an internally mounted 10m radius gold coated mirror and an externally mounted 5m radius gold coated mirror. The mirrors were separated by 2m, and a 1 mm central pinhole in the internally mounted mirror provided the output coupling from the cavity. The multimode output from a Lumonics 203 grating tuned CO_2 TEA laser was weakly focused (to match the dimensions of the square tube) and introduced into the OPML cell from an external mirror located below the axis of the OPML cavity. The angle of entry was chosen to be the minimum angle which would give symmetric pumping of the cell by reflection from the internally mounted mirror and the surfaces of the tube. This entrance angle was found to produce the maximum OPML output in a similar room temperature device.[7] The CO_2 pump energy introduced into the OPML cell on the lines of interest was ~ 4J, of which approximately 40% was concentrated in an initial 60 ns FWHM gain-switched 'spike'.

The performance of the OCS and CF_4 OPMLs in the laser system described above is illustrated in Fig.2 which shows OPML output energy vs pressure at several gas temperatures. For the OCS OPML, the curves correspond to operation on the Q(4) transition only, operation of the P(5) transition was prevented by the intracavity Brewster window. In both Figs.2a and 2b the inner curves correspond to pressure variation at a constant temperature while the outer curve in each figure corresponds to laser operation in a saturated vapour of the gas. For both lasers, Fig.2 illustrates that the maximum output energies are achieved at the SVP limiting temperature. In more recent experiments where an intracavity beam-splitter was used to couple out energy from the OPML cavity, maximum energies of 1.6 and 0.75 mJ were achieved from CF_4 and OCS respectively with the same cell as described above. These energies correspond to specific energy extractions of 10 $\mu J\ Torr^{-1} cm^{-3}$ for CF_4 and 7.5 $\mu J\ Torr^{-1} cm^{-3}$ for OCS at 3.5 J CO_2 multi-mode input.

The effect of cooling an OPML is two-fold. Firstly, it reduces the thermal population initially residing in the lower laser level which can be $\geq$ 10% of the ground state population at room temperature for CO_2 pumped OPMLs. This reduction improves the OPML efficiency and the maximum pressure at which the OPML can operate. Secondly, cooling changes the initial thermal population of the lower level of the optically pumped transition. This change can be either positive or negative, and will be directly reflected in an increase or decrease in the energy extracted from the OPML as discussed below.

The behaviour of output energy vs pressure for the OCS OPML at room temperature has previously been described in terms of a detailed rate equation model.[8] However a simple semi-quantitative description of the curves in Fig.2, in particular of the behaviour of maximum operating pressure with temperature, may be expressed in terms of the population inversion ($n_u - (g_u/g_\ell)n_\ell$, where the usual notation has been employed) established before laser action occurs. The population n_ℓ will increase linearly with pressure (ie will maintain its equilibrium thermal population) while n_u will increase only sublinearly with pressure. Over a wide pressure range these populations may be written*

$$n_u(t) = g_u N_t \{Q_v Q_R (2 + [W(t) \tau_R]^{-1})\}^{-1} \exp(-Ep/kT) \quad \ldots(1)$$

$$n_\ell = g_\ell N_t (Q_v Q_R)^{-1} \exp(-E_\ell/kT) \quad \ldots(2)$$

where we make the assumptions, justified (at least for OCS) by the analysis of the room temperature OCS OPML,[8] that the population n_u maintains a steady-state value with respect to the CO_2 laser stimulated pumping rate W(t) (which has the same time dependence as the intensity of the CO_2 pumping pulse) and that over the period prior to OPML action (typically $\leq$ 200 ns) depletion of the ground vibrational manifold is negligible and filling of the excited vibrational manifolds containing the upper and lower OPML levels is not significant. In Eqns.(1) and (2) the subscript 'p' refers to the lower level of the pump transition and g and E refer to the degeneracy and energy of the level specified by the

---

* These populations are total values for all states having the same vibrational and rotational quantum numbers. Where the degeneracies of these states are lifted, the expressions need to be modified.

subscript. N_t is the total density of molecules, Q_v and Q_R are the vibrational and rotational partition functions respectively and τ_R is the rotational relaxation time of a level (assumed equal for the three levels involved).

Fig.3 plots n_u and $(g_u/g_\ell)n_\ell$ immediately prior to OPML action, for the OCS OPML as a function of pressure and at two of the temperatures for which data is presented in Fig.2(a). The curves were calculated using Eqns.(1) and (2). A constant value $\tilde{W}$ was assumed for W(t) in Eqn.(1), and the value was chosen to give an intersection of the 296K curves at a pressure corresponding to the maximum observed from the laser at this temperature. The simplifying assumption of a constant pumping rate $\tilde{W}$ is justified in the spirit of the overall approximations employed here on the grounds that strong OPML emission occurs only after optical pumping by the gain switched 'spike' of the CO_2 laser is complete, ie the term $\tilde{W}$ corresponds to optical pumping by the 'tail' of the CO_2 laser pulse which is relatively flat and extends for several μs. Further, auxiliary experiments in which an absorbing cell of the lasant gas was placed in the pump beam between the CO_2 pump laser and OPML cell demonstrated that depletion of the pump radiation over the 1m length of the OPML cell could be neglected and did not contribute significantly to the fall-off in OPML output at higher pressures. Of the other parameters included in the calculations leading to the curves in Fig.3, Q_R was calculated using the semi-classical expression for a linear molecule,[9] Q_v was calculated by summing the individual Boltzmann terms for each individual vibrational manifold,[9] and E_p and E_ℓ were calculated using published assignments for the OCS OPML levels[6] (giving E_p = 6 cm^{-1}, E_ℓ = 532 cm^{-1}). The experimental value for τ_R of 29 ns at 1 Torr and 300K[10] was, in the absence of better data, scaled to other temperatures by assuming a temperature independent cross section for the rotational relaxation process. The validity of this assumption is examined later.

A direct comparison of the curves in Figs.2a and 3 shows a general qualitative agreement in the temperature dependence of the maximum output energy and operating pressure. In particular, it can be shown that the maximum operating pressure (P_{max}) observed experimentally corresponds to the pressure at which the values of n_u and n_ℓ (predicted by Eqns.(1) and (2)) are equal. Thus, using Eqns.(1) and (2), the

general expression for P_{max} is given by

$$P_{max} = \tilde{W} (\tau_R)_{300K} (T/300)^{\frac{1}{2}} \left\{ \exp [(E_\ell - E_p)/kT] - 2 \right\} \text{Torr} \quad \ldots(3)$$

where $(\tau_R)_{300K}$ is the rotational relaxation time at 300K and 1 Torr pressure. In Fig.4, the maximum operating pressure observed experimentally is compared to the predictions of eqn.(3) as a function of temperature, the value of $\tilde{W}$ being adjusted (as explained above) to give agreement at 294K.

The deviation between observed and experimentally measured maximum operating pressures for the OCS OPML can readily be explained in terms of the reduced OPML gains at higher pressures resulting from collisional broadening of the laser transition. Collisional broadening and Doppler broadening of the laser transition become comparable at 300K for pressure exceeding 2 Torr in OCS and 4 Torr in CF_4.* The effect of collisional broadening in OCS is illustrated by the dashed curves in Fig.3 which show the calculated gain vs pressure for the two temperatures corresponding to the other curves in this figure. The reduced gains result in an increased laser build-up time which increases the importance of such deleterious effects as vibrational relaxation between the upper and lower laser levels. Under lower gain conditions the effects of losses in the OPML cavity, especially 'warm' gas at the ends of the OPML cell, also become more important and prevent the maximum theoretical operating pressure from being achieved. Nevertheless the operating pressures achieved in these experiments are the maximum values reported for both the OCS and CF_4 OPMLs. Fig.5 shows the maximum operating pressure vs temperature for the CF_4OPML, showing a rapid rise in maximum operating pressure at the lowest possible temperatures. However, a lack of available quantitative information on the energy levels involved in CF_4 OPML presently precludes a comparison with theoretical predictions from being made. There is also the possibility in CF_4 at higher pressures of strong ground state absorption at the OPML wavelength.

---

* These values are calculated using pressure broadening coefficients of 11 MHz $Torr^{-1}$ for OCS[8] and 6 MHz $Torr^{-1}$ for CF_4.[11]

A consequence of the reasonable agreement between theory and experiment illustrated in Fig.4 is that it supports an assumption made in obtaining Eqn.(3) that the collisional cross section for rotational relaxation in OCS is independent of temperature. Any strong temperature dependence of this cross section would directly modify the expression for P_{max} in Eqn.(3). For collisions associated with electrostatic interactions of molecules (eg dipole-dipole type) the calculated P_{max} would be lower than the value given by eqn.(3) and, taking into account the effects of lower OPML gains at higher pressures, would appear inconsistent with the experimental results.

Assuming then a temperature independent cross section for rotational relaxation, it follows that at a constant pressure the rotational relaxation time will vary as $T^{\frac{1}{2}}$. Consequently, the experimental curves in Figs.4 and 5 illustrate that cooling produces large improvements in the maximum rotational rate that can be maintained during OPML operation. Increases over room temperature values in the maximum tolerable rotational relaxation rate of 3.5 for OCS and of 6.3 for CF_4, may be deduced from Figs.4 and 5. This finding indicates the importance of cooling to obtain line-tunable OPML operation, since such operation relies on rotational relaxation to distribute population from the directly pumped level to neighbouring levels.

The importance of laser gain rather than population inversion in determining the dependence of output energy on operating conditions from a given OPML is reflected in the temperature dependence of the optimum OPML pressure for maximum output energy. As seen in Fig.2, for both the OCS and CF_4 OPMLs this optimum pressure remains approximately constant, decreasing slightly with reduced temperature. A similar result was obtained for the 12.08 μm NH_3 OPML.[5] Likewise, the maximum gain (and <u>not</u> the maximum population inversion) occurs at a pressure which decreases slowly with decreasing temperature as a result of the Doppler linewidth of the OPML transition decreasing and the collisional broadening coefficient increasing (as explained above).

In Fig.6 the OPML pulse energy obtained at the optimum (temperature dependent) pressure is plotted against operating temperature for the OCS and CF_4 OPMLs. These curves reflect both a decreasing lower laser level (thermal) population and an increasing lower pump level (thermal) population with decreasing temperature. The latter

effect becomes particularly important at lower temperatures. In this respect it is interesting to note that the lower level of the pump transition for CF_4 has been assigned as being around J = 32,[4] and the fractional population of a level in this vicinity would begin to decrease slowly for T ≤ 200K. This may explain the observed independence of output energy with temperature for temperatures between 100K and 150K. In the case of the OCS OPML no such reduction in the fractional population of the lower J = 5 pump level occurs, and the output energy from the laser increases up to the lowest possible operating temperatures. In the context of interpretation of the variation in OPML output energy with temperature, recently published results for the C_2D_2 OPML[12] obtained using the OPML cell described above helped to identify hot-band pump transitions as well as broadly confirming assignments of various lower levels of the other pump transitions.

In conclusion, a LN_2 cooled OPML cell has been described and results of low temperature operation of the OCS 19 μm OPML and the CF_4 16 μm OPML have been presented and analysed. The results clearly illustrate the improvements that can be achieved by operating OPMLs at low temperatures, in particular in increasing the laser output energy and the possibility of line tuning at high pressures.

REFERENCES

1. R.M. Osgood, Appl.Phys.Lett.28, 342 (1976)

2. M.I. Buchwald, C.R. Jones, H.R. Fetterman and H.R. Schlossberg, Appl.Phys.Lett.29, 300 (1976)

3. J.J. Tiee and C. Wittig, Appl.Phys.Lett.30, 420 (1977)

4. J.J. Tiee and C. Wittig, J.Appl.Phys.49, 61 (1978)

5. T. Yoshida, K. Miyazaki and K. Fujisawa, Japan J.Appl.Phys.17, 747 (1978)

6. H.R. Schlossberg and H.R. Fetterman, Appl.Phys.Lett.26, 316 (1975)

7. R.C. Harrison and F.A. Al-Watban, Opt.Comm.20, 225 (1977)

8. E. Armandillo and J.M. Green, J.Phys.D.11, 421 (1978)

9. G. Herzberg, 'Molecular Spectra and Molecular Structure' Vol.II, Pub. D. Van Nostrand Co.Ltd., London 1945, pp.503-506.

10. Yu. R. Kolomüskü, V.S. Letokhov and O.A. Turnanor, Sov.J.Quantum Elect.6, 959 (1976)

11. D.N. Travis, private communication.

12. H.N. Rutt and J.M. Green, Opt.Comm.26, 422 (1978)

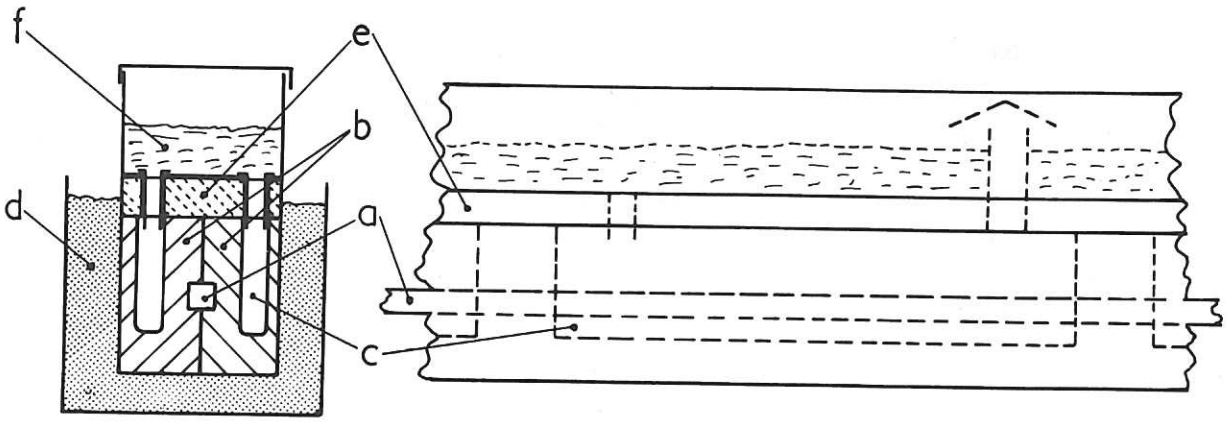

Fig.1 Cooled OPML cell. (a) tube containing OPML gas, (b) brass blocks, (c) cooling channels, (d) thermal insulation, (e) insulating block, (f) LN_2 tank.

(a)

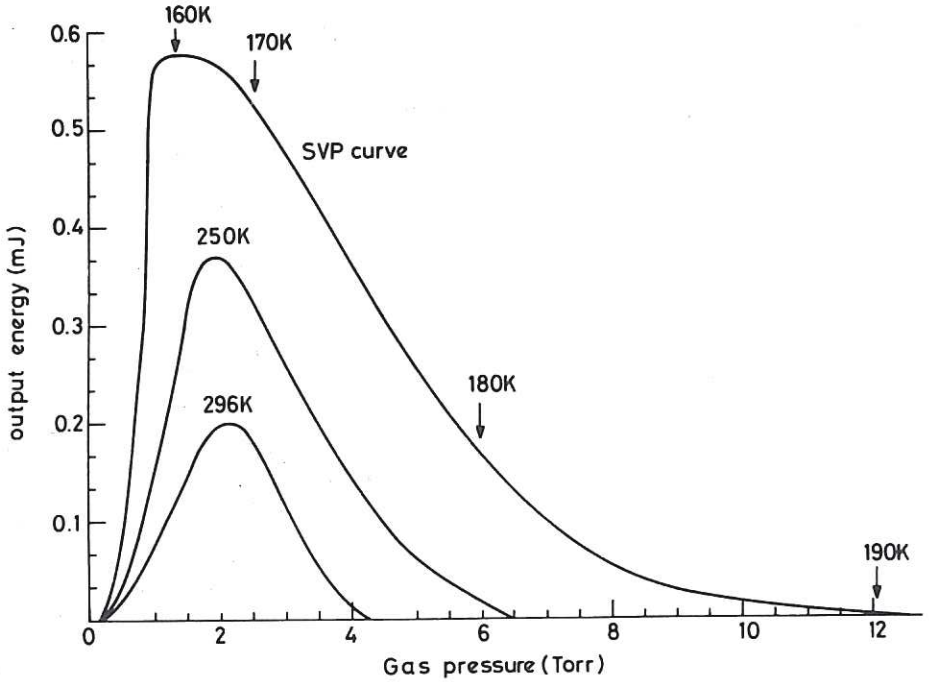

(b)

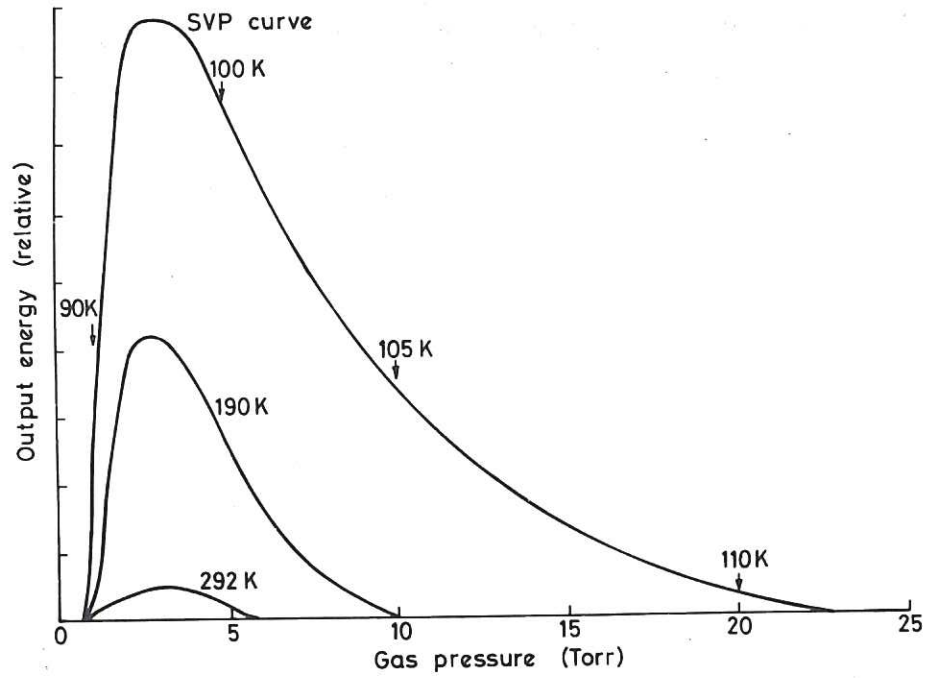

Fig.2 Output energy vs gas pressure at various temperatures for (a) the 19μm OCS OPML, (b) the 16μm CF_4 OPML.

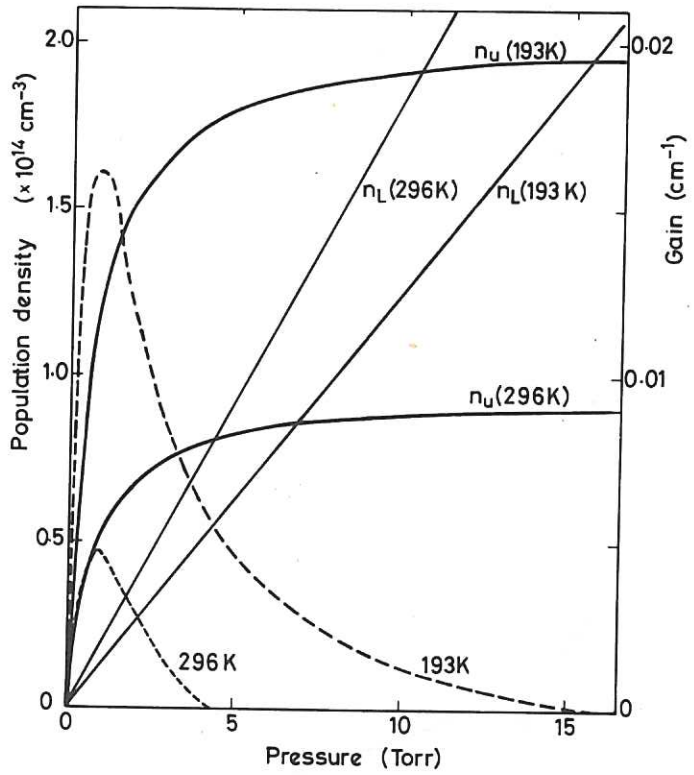

Fig.3 Theoretical curves for the population density (solid curves) and gain (dashed curves) immediately prior to laser action as a function of gas pressure for the OCS OPML.

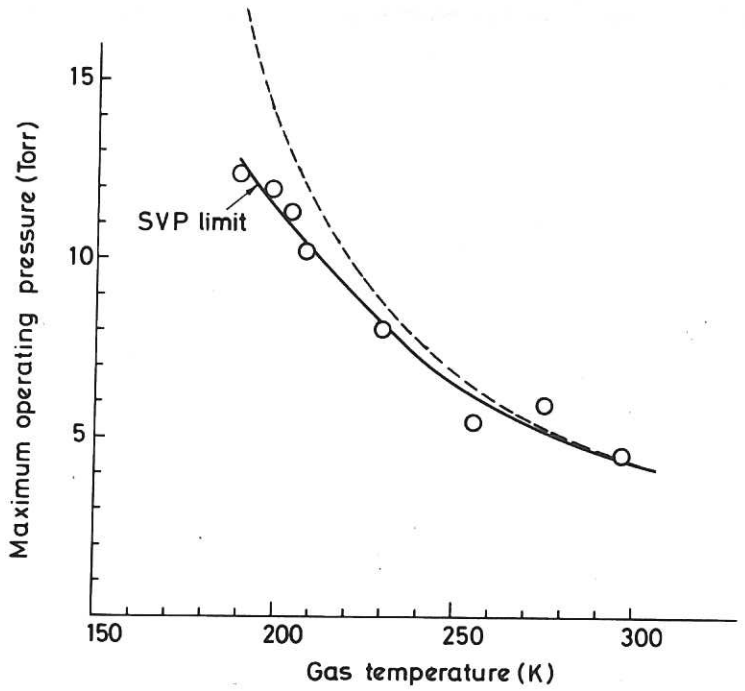

Fig.4 Maximum operating pressure vs gas temperature for the OCS OPML. Solid curve is the best fit to experimental points, dashed curve calculated using Eqn.(3).

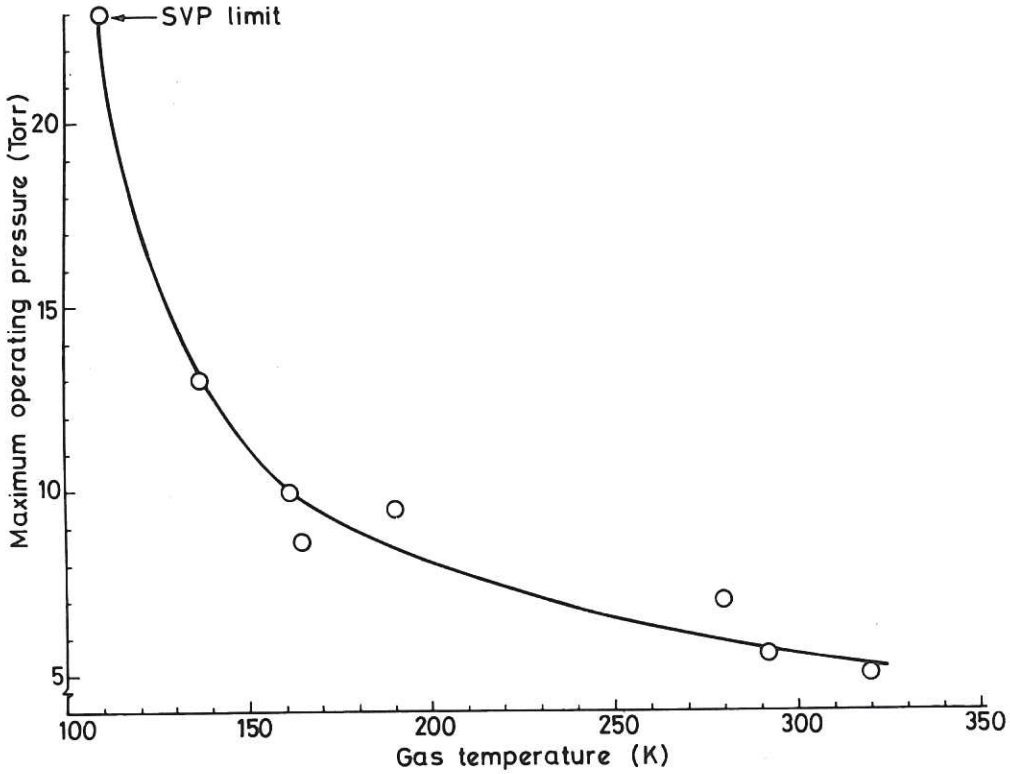

Fig.5 Maximum operating pressure vs gas temperature for the CF_4 OPML.

(a)

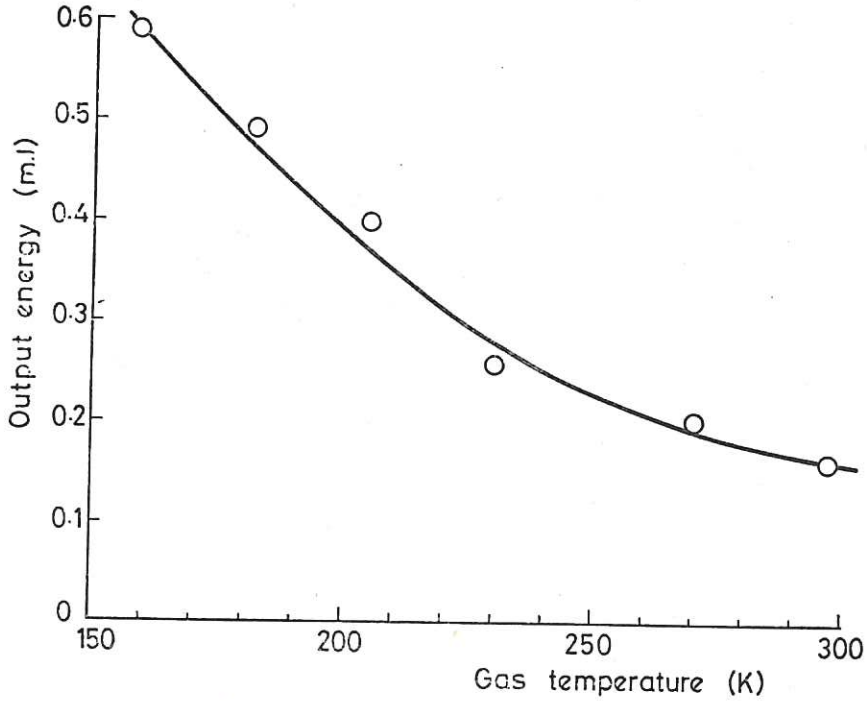

(b)

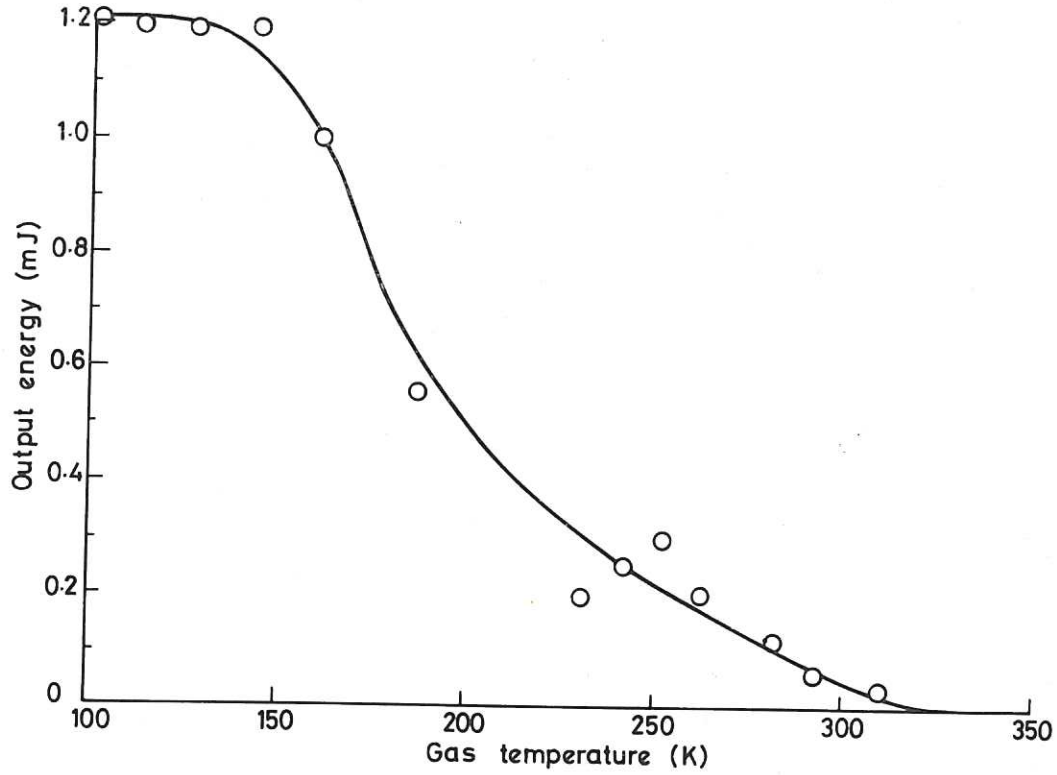

Fig.6 Maximum output energy vs gas temperature for (a) the 19μm OCS OPML, (b) the 16μm CF_4 OPML.